Magnetic Resonance Imaging 98 (2023) 97–104

Contents lists available at ScienceDirect

Magnetic Resonance Imaging

journal homepage: www.elsevier.com/locate/mri

Deep learning for improving ZTE MRI images in free breathing

D. Papp [a,*], Jose M. Castillo T [a], P.A. Wielopolski [a], P. Ciet [a,b], Jifke F. Veenland [a,c], G. Kotek [a], J. Hernandez-Tamames [a]

[a] Department of Radiology and Nuclear Medicine, Erasmus Medical Centre, Rotterdam, the Netherlands
[b] Department of Pediatric Pulmonology and Allergology, Erasmus Medical Centre - Sophia Children's Hospital, Rotterdam, the Netherlands
[c] Department of Medical Informatics, Erasmus Medical Centre, Rotterdam, the Netherlands

ARTICLE INFO

Keywords:
Magnetic resonance imaging
Zero TE
Lung
Fully convolutional neural networks

ABSTRACT

Introduction: Despite a growing interest in lung MRI, its broader use in a clinical setting remains challenging. Several factors limit the image quality of lung MRI, such as the extremely short T2 and T2* relaxation times of the lung parenchyma and cardiac and breathing motion. Zero Echo Time (ZTE) sequences are sensitive to short T2 and T2* species paving the way to improved "CT-like" MR images. To overcome this limitation, a retrospective respiratory gated version of ZTE (ZTE4D) which can obtain images in 16 different respiratory phases during free breathing was developed. Initial performance of ZTE4D have shown motion artifacts. To improve image quality, deep learning with fully convolutional neural networks (FCNNs) has been proposed. CNNs has been widely used for MR imaging, but it has not been used for improving free-breathing lung imaging yet. Our proposed pipeline facilitates the clinical work with patients showing difficulties/uncapable to perform breath-holding, or when the different gating techniques are not efficient due to the irregular respiratory pace.

Materials and methods: After signed informed consent and IRB approval, ZTE4D free breathing and breath-hold ZTE3D images were obtained from 10 healthy volunteers on a 1.5 T MRI scanner (GE Healthcare Signa Artist, Waukesha, WI). ZTE4D acquisition captured all 16 phases of the respiratory cycle. For the ZTE breath-hold, the subjects were instructed to hold their breath in 5 different inflation levels ranging from full expiration to full inspiration. The training dataset consisting of ZTE-BH images of 10 volunteers was split into 8 volunteers for training, 1 for validation and 1 for testing. In total 800 ZTE breath-hold images were constructed by adding Gaussian noise and performing image transformations (translations, rotations) to imitate the effect of motion in the respiratory cycle, and blurring from varying diaphragm positions, as it appears for ZTE4D. These sets were used to train a FCNN model to remove the artificially added noise and transformations from the ZTE breath-hold images and reproduce the original quality of the images. Mean squared error (MSE) was used as loss function. The remaining 2 healthy volunteer's ZTE4D images were used to test the model and qualitatively assess the predicted images.

Results: Our model obtained a MSE of 0.09% on the training set and 0.135% on the validation set. When tested on unseen data the predicted images from our model improved the contrast of the pulmonary parenchyma against air filled regions (airways or air trapping). The SNR of the lung parenchyma was quantitatively improved by a factor of 1.98 and the CNR lung- blood, which is indicating the visibility of the intrapulmonary vessels, was improved by 4.2%. Our network was able to reduce ghosting artifacts, such as diaphragm movement and blurring, and enhancing image quality.

Discussion: Free-breathing 3D and 4D lung imaging with MRI is feasible, however its quality is not yet acceptable for clinical use. This can be improved with deep learning techniques. Our FCNN improves the visual image quality and reduces artifacts of free-breathing ZTE4D. Our main goal was rather to remove ghosting artifacts from the ZTE4D images, to improve diagnostic quality of the images. As main results of the network, diaphragm contour increased with sharper edges by visual inspection and less blurring of the anatomical structures and lung parenchyma.

Conclusion: With FCNNs, image quality of free breathing ZTE4D lung MRI can be improved and enable better visualization of the lung parenchyma in different respiratory phases.

* Corresponding author.
E-mail address: d.papp@erasmusmc.nl (D. Papp).

https://doi.org/10.1016/j.mri.2023.01.019
Received 8 August 2022; Received in revised form 7 November 2022; Accepted 14 January 2023
Available online 18 January 2023

1. Introduction

Computed tomography (CT) has been historically favored over magnetic resonance (MR) when imaging the lung and airways due to technical challenges inherent to lung structure and the difficulty obtaining high-quality MR images of the chest [1]. MR is a non-ionizing technique with potential for robust functional and structural assessment in a single examination [2]. Nonetheless, it is more time consuming to obtain high quality MR images of lung parenchyma compared to other anatomical regions [3]. This is mainly due to low proton density of lung tissue, susceptibility differences between tissue and air [4] and motion of the heart and lung parenchyma. These issues have a strong effect on gradient echo MR sequences leading to a rapid signal decay, low signal-to-noise ratio (SNR), and therefore low image quality.

To minimize these issues, new pulse sequences have been introduced enabling higher SNR and improving image quality, namely Ultrashort Echo Time (UTE) [5,6] and Zero Echo Time (ZTE) sequences [4,7]. UTE/ZTE sequences can capture fast decaying signals from lung parenchyma using echo time (TE) in the order of microseconds instead of milliseconds. According to a recent study comparing UTE and ZTE lung MR images, ZTE performs better than UTE for the detection of lung parenchyma signal and the visualization of intrapulmonary structures [8] with optimized parameters used for each sequence. To avoid motion artifacts, images are often acquired at end of expiration, being the longest motionless phase in the respiratory cycle and therefore leading to significant decreases in respiratory motion artifacts [9]. For this, either the patients need to adjust their breathing to the data acquisition (in the form of breath holding), or vice versa, the scanner is prospectively adjusted to free-breathing using respiratory triggering or navigators [9,10]. By adding a time dimension to volume data, it is possible to acquire both the inspiratory and the expiratory phases of the respiratory cycle. This can be performed using retrospective gating with a dynamic four-dimensional (4D) scan. ZTE4D (*GE Healthcare, Waukesha, WI, USA*) is a retrospective respiratory gated version of ZTE which can obtain images in sixteen ($n = 16$) different respiratory phases during free breathing [11]. However, this technique shows some limitations in clinical settings. For instance, from all the 16 respiratory phases only the end-expiratory ones give acceptable image quality. Inspiratory phases present higher level of noise, motion artefact from diaphragm movement and blurring around the edges of the tissues that limit their diagnostic use. Patients with chronic obstructive pulmonary disease (COPD), asthma and young children also have problem to hold their breath, with higher chances of motion artifacts.

To overcome these problems and to improve image quality, artificial intelligence, more specifically machine learning techniques can be used. Deep learning (DL) is a subset of machine learning methods that uses multiple layers to progressively extract high-level features from raw input. DL is a promising technique in the medical imaging field, especially for image classification, lesion detection, segmentation and image quality improvement [12] . Within the DL methods, convolutional neural networks (CNN) show a remarkable performance in image segmentation, and classification [13,14]. In particular fully convolutional neural networks (FCNN) - a neural network that only performs convolutions and subsampling or upsampling operations - can efficiently learn to make predictions for pixel-wise tasks like semantic segmentation and image denoising [15].

To our knowledge, the potential of FCNNs to remove motion artifacts and denoising has not been tested in chest ZTE4D MRI imaging to date. The purpose of our study was to improve the image quality of ZTE4D images using a post-processing pipeline with a FCNN trained algorithm based on breath-hold ZTE (ZTE-BH) images, which were used as reference. We demonstrate the capability of our method to reconstruct all 16 respiratory phases of ZTE4D with equally acceptable image quality. Our proposed pipeline facilitates the clinical work with patients showing difficulties/uncapable to perform breath-holding, or when the different gating techniques are not efficient due to the irregular respiratory pace.

Table 1
Acquisition parameters [11].

Sequence	ZTE4D (vol)	ZTE3D BH (vol)
Acquisition plane	Coronal	Coronal
TR/TE (ms/μs)	1.4/2	1.25/2
flip angle (°)	1	2
RF	Non-selective	Non-selective
In-plane matrix	150 × 150	150 × 150
k-space trajectory	Radial	radial
In-plane Field-of-view(FOV)	34	34
RecFOV	-	-
Actual voxel resolution (mm^3)	2.2 × 2.2 × 2.2	2.2 × 2.2 × 2.2
	110	110
	2.2	2.2
Receiver bandwidth (KHz)	50	62.5
Number of averages	7	1
Number of phases	16	1
No. of readout spokes per segment	64	200
Physiological triggering	Retrospective pneumobelt	BH
Scan time (*sec*) RR = 20	3 min 10s	20s

2. Materials and methods

In 4D ZTE, a retrospective soft gating method was used for motion correction and image reconstruction as follows. *k*-space data along with physiological signals derived from respiratory bellows were collected during the whole respiratory cycles. The k-space data were binned into four respiratory motion states based on physiological signals. For each respiratory motion state, the k-space data were weighted depending on the respiratory displacement from an ideal target physiological signal. The corresponding image volume was then reconstructed [11].

On the ZTE4D images in respiratory phases not near end-expiration, the most problematic artifacts are: the motion artefact of the diaphragm, blurring edges of tissues (most importantly of intrapulmonary vessels) and higher noise level of the lung parenchyma. A FCNN has been trained to learn and remove artifacts.

2.1. Volunteers and imaging

The study including healthy volunteers scanning was approved by the local Institutional Review Board (MEC2018–134, MEC2018–002). Written informed consent was obtained from all subjects before MR scans. From March 2019 to May 2020 the volunteers underwent chest MRI. MRI scans were performed on a 1.5 T scanner (*Signa Artist, GE Healthcare, Waukesha, WI, USA*) without contrast agent. The MRI protocol consisted of a retrospectively reconstructed multi-phase radial ZTE3D scan (ZTE4D) and a 20 s breath-hold radial ZTE3D (ZTE3D-BH) using a 32-channels body coil. Both sequences were optimized for Proton-Density (PD) weighting. All scans used 3D grad warping to compensate for gradient non-linearities within the large field-of-views (FOV) acquired. Details of the acquisition parameters are presented in Table 1.

ZTE4D acquisition captured the maximum16 phases along the respiratory cycle to achieve the highest possible time resolution. We compared ZTE4D to ZTE-BH, which was used as 'ground-truth' to identify possible artifacts for each respiratory phase. For obtaining comparable images between the 2 acquisitions, we obtained ZTE-BH at five ($n = 5$) different inflation levels ranging from full expiration to full inspiration. To match the tidal breathing respiratory excursion, the volunteers were instructed to take consecutively one, two and three small breaths and hold the inspiratory positions until scanning was completed. The middle 3 inspiratory levels of ZTE-BH that matched the excursion of the reconstructed phases of the ZTE4D acquisitions were chosen for comparison. Full inspiration (total lung capacity) and full expiration (residual volume) were excluded, as during tidal breathing the volunteers usually do not reach these respiratory phases.

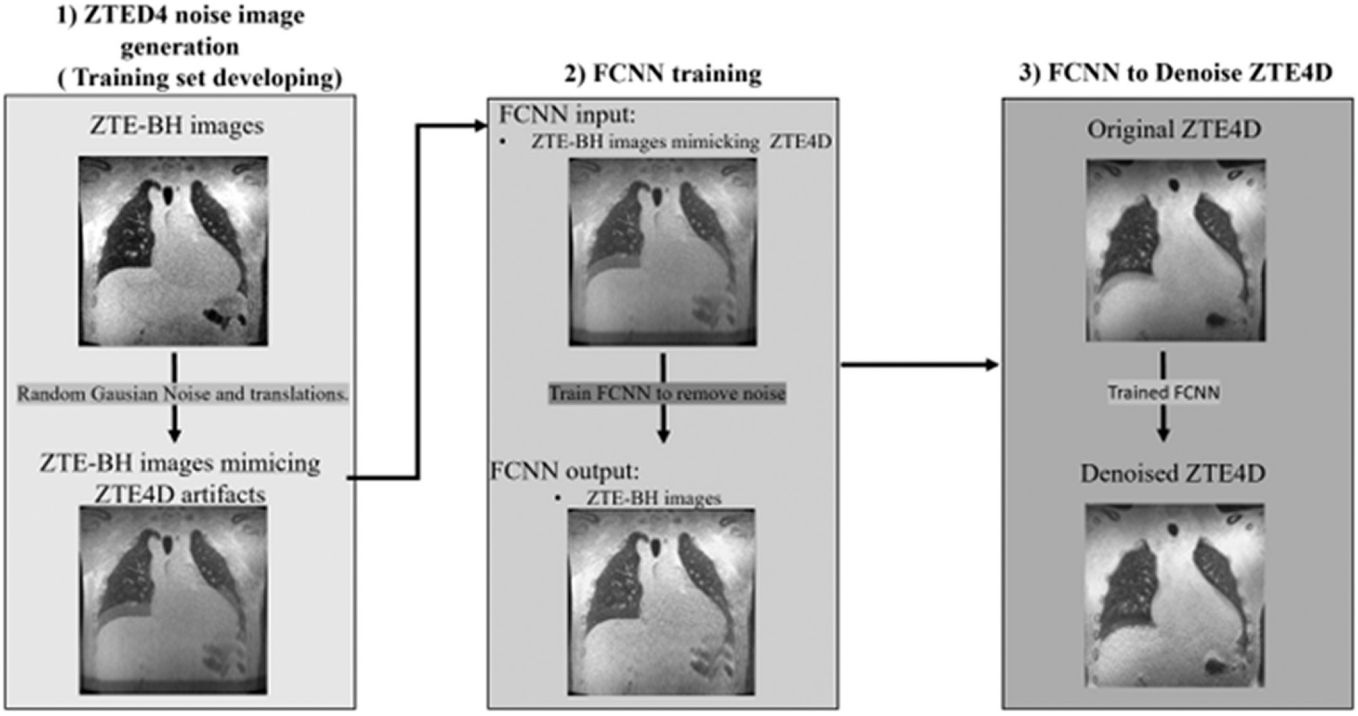

Fig. 1. Flow diagram of the proposed framework. The first step was the modification of the original breath-hold images, followed by the training of the FCNN, then the denoising of the original ZTE4D images.

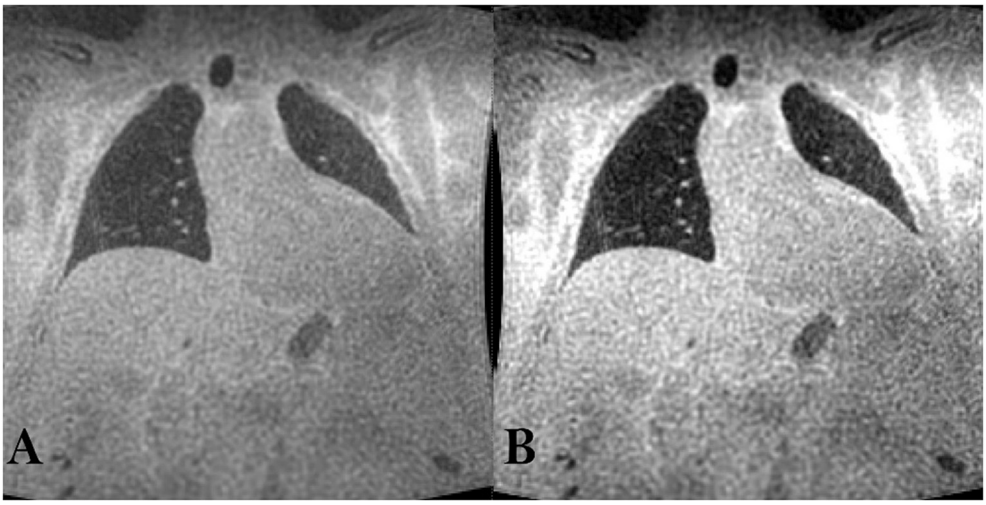

Fig. 2. Example of enhancing original ZTE-BH images with increased contrast level and wavelet denoising. A) native image and B) is the enhanced version.

2.2. The preparation and image reconstruction pipeline

Our set-up consists of three major components, which are summarized in Fig. 1. The first component aims to reproduce the artifacts on the ZTE-BH images as they are regularly present in free breathing ZTE4D images. The second component uses the modified (as explained in the 'training set generation/creation' section) ZTE-BH as input for training the FCNN which gives the artefact free image as output. The last component takes the network trained on ZTE-BH to remove the artifacts from free-breathing ZTE4D. The details of each component are explained in the following sections.

1) Training set generation/creation

For the purpose of creating a training dataset for the neural network, we modified the ZTE-BH image data (Fig. 1) to simulate the artifacts of ZTE4D images. The power of the noise is often estimated from the standard deviation of the pixel signal intensity in an image region with no signal [16]. To get lower SNR, we added Gaussian noise to the real and imaginary components and performed image transformations (translations, rotations) to imitate the effect of motion in the respiratory cycle and motion artefact from varying diaphragm positions. Each respiratory phase has different standard deviation of the noise (difference in SNR) and different amplitude of the translation (shadowing artifacts of the diaphragm on the ZTE4D images). To account for these differences by keeping only anatomically possible scenarios on the ZTE4D images, we used different random noise levels and different weight parameters of the artifacts on each slice. More specifically; between a given range

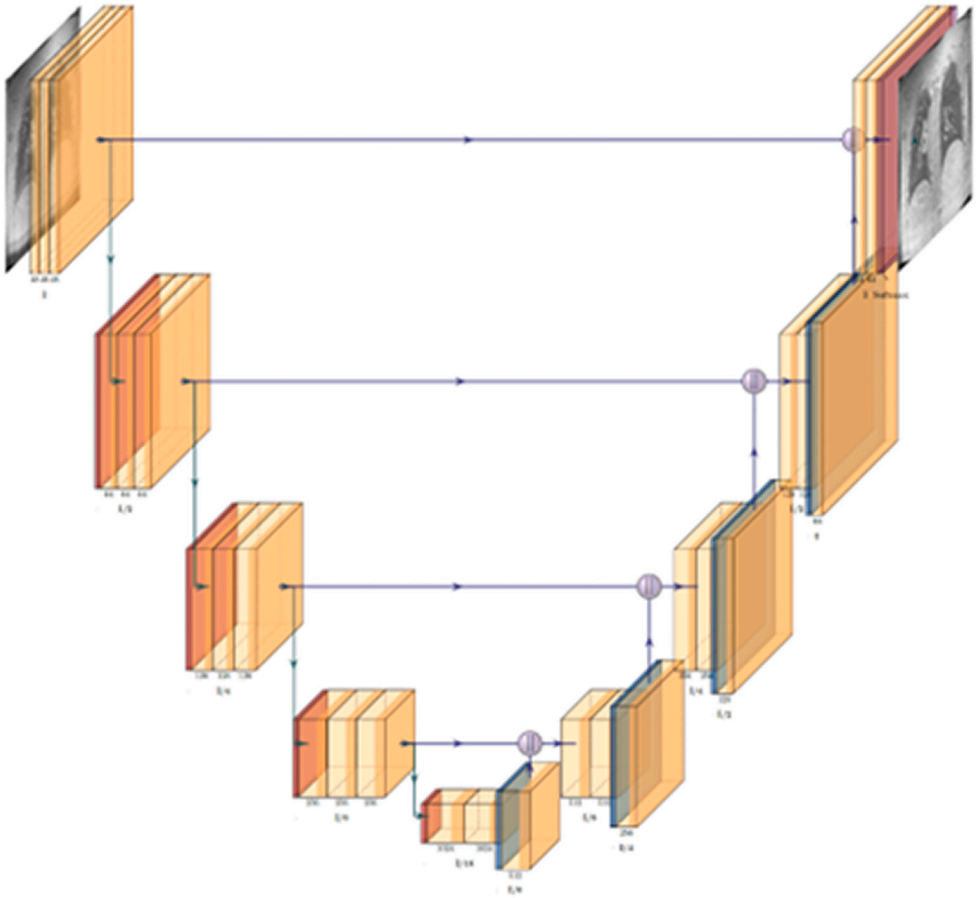

Fig. 3. Architecture of our model (a modification taken from [15]). The network uses a 3 × 3 convolution kernel size.

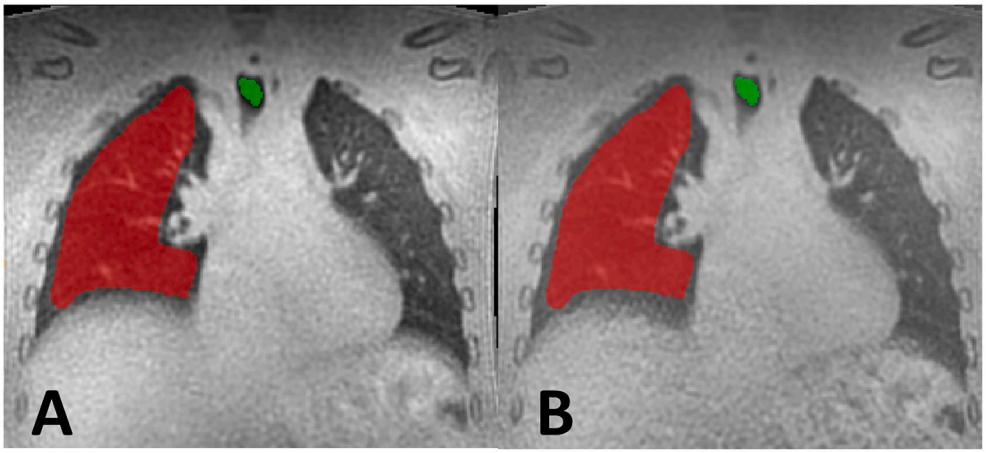

Fig. 4. Positioning of the ROIs to calculate SNR values. The mean signal intensity (SI) of the red area was divided by the standard deviation (STD) of the green area. On the left (A) the original image and on the right the predicted images. (For interpretation of the references to colour in this figure legend, the reader is referred to the web version of this article.)

we changed the kernel and standard deviation values of the Gaussian noise and choose randomly from 60 different shift values (used values to be found in the provided github repository). To mimic the diaphragm movement, we randomly applied the shift filter either one or two times. With this approach, we left the possibility to have images which did not change from the original at all (mimicking those end-expiratory phases captured properly), and the ones representing the worst possible scenarios. For each original ZTE-BH slice one ZTE4D like image were constructed. Each ZTE-BH phase contained 110 slices (330 slices per volunteer were captured). After clearing the data from slices not containing any anatomical information, 1000 ZTE breath-hold slices with variety of artifacts were used for training.

In order to increase the efficiency of the network, we enhanced the ground truth (original ZTE3D-BH) images without changing any of their characteristics by increasing the contrast using wavelet denoising [17]. Fig. 2 shows an example of the original and the enhanced BH images.

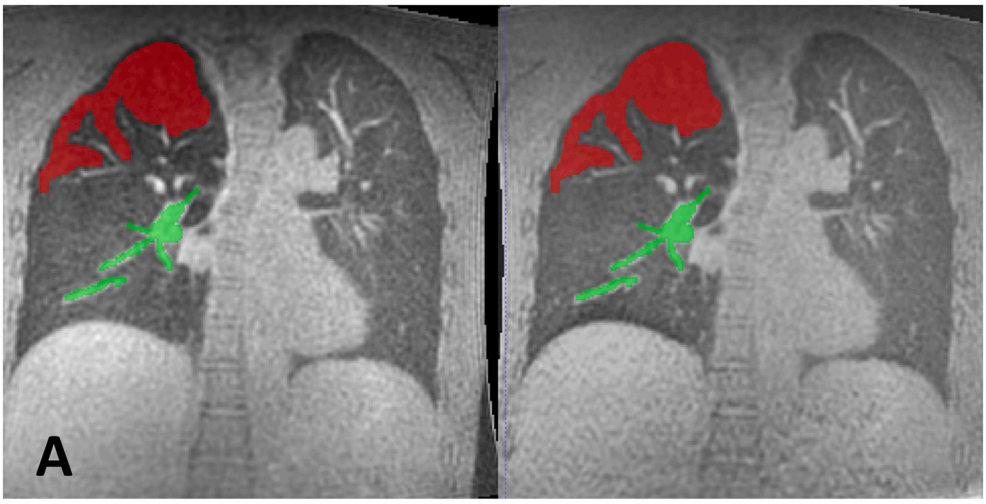

Fig. 5. Positioning of the ROIs to calculate CNR values. The mean SI of the red area was subtracted from the mean SI of the green area, divided by the STD of the red area. A is the original image and B the predicted. (For interpretation of the references to colour in this figure legend, the reader is referred to the web version of this article.)

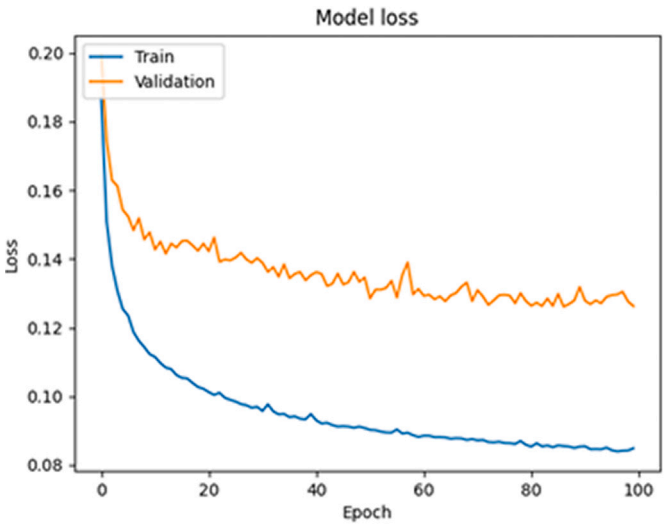

Fig. 6. MSE loss funtion of the validation and training sets.

Table 2
Comparison of SNR of the lung parenchyma and CNR of the lung parenchyma and blood between the original and the improved dataset (mean ± standard deviation).

	Original ZTE4D	Predicted ZTE4D
SNR	479.55 ± 96.15	952.95 ± 254.04
CNR	10.42 ± 3.53	10.87 ± 3.70

2) Fully convolutional neural network Training

2.1 FCNN input

The ZTE4D like ZTE-BH images obtained in the previous step were used as input for the FCNN. The network's task was to predict the enhanced ZTE-BH image as output. Therefore, the network would learn suited features to remove the breathing motion artefact and blurring effects. The network's architecture is described in Section 2.2. The training dataset consisting of ZTE-BH images of 10 volunteers was split into 8 volunteers for training, 1 for validation and 1 for testing.

2.2 Network architecture

We followed the same architecture as in Souza and Frayne [18] with the modification of removing the second U-net. Our network contains three successions of three 2D convolutions with a 3 × 3 kernel size, followed by a rectified linear unit each and a max pooling of 2 × 2. A last succession of three consecutive 2D convolutions with up-sampling. A concatenation with the corresponding computed featured map from the down-sampling part was performed after up-sampling. In the final layer, a 2D convolution having 1 × 1 kernel size was used to map computed features to restore the modified image. In each convolution layer, appropriate padding was used. A schematic representation of the used CNN is shown in Fig. 3. The original code, and the code used in our experiments can be found in Github [19,20].

The training of the network was implemented in Keras (version 2.0.2) with Tensor Flow (version 1.0.1) as backend in Python (version 3.5.3). The training and prediction were performed on a GeForce GTX TITAN Xp GPU (NVIDIA). The loss function during training was mean squared error (MSE) and optimized using Adam optimizer [14] with a learning rate of 0.01. The total number of epochs was set to 500. The output of the trained network was a 256 × 256 image.

3) FCNN to remove artifacts.

As the last step we tested the trained network on the unseen original ZTE4D data of six (n = 6) volunteers (age range 20–52, median 28). Afterwards, the images predicted by the network were quantitatively evaluated in terms of SNR, CNR and the artifacts were qualitatively evaluated by visual inspection.

2.3. *Quantitative assessment*

To evaluate the ability of the network in detecting lung parenchyma signal and depict different structures (e.g alveoli, bronchi), the signal intensity (SI) of the parenchyma was measured. Additionally, unconventional SNR values were calculated, where regions of interest (ROIs) were drawn in the lung parenchyma and in the tracheal lumen air. The ROI in the lung parenchyma was carefully positioned and sized on the original scans as it covered the whole area, leaving out major vessels; the ROIs were subsequently copied to the predicted slices, evaluated per subject (Fig. 4). The SNR of the lung parenchyma was compared between the original images and the predicted ones. SNR was calculated as the mean SI of the measured structure divided by the standard deviation (STD) of the trachea:

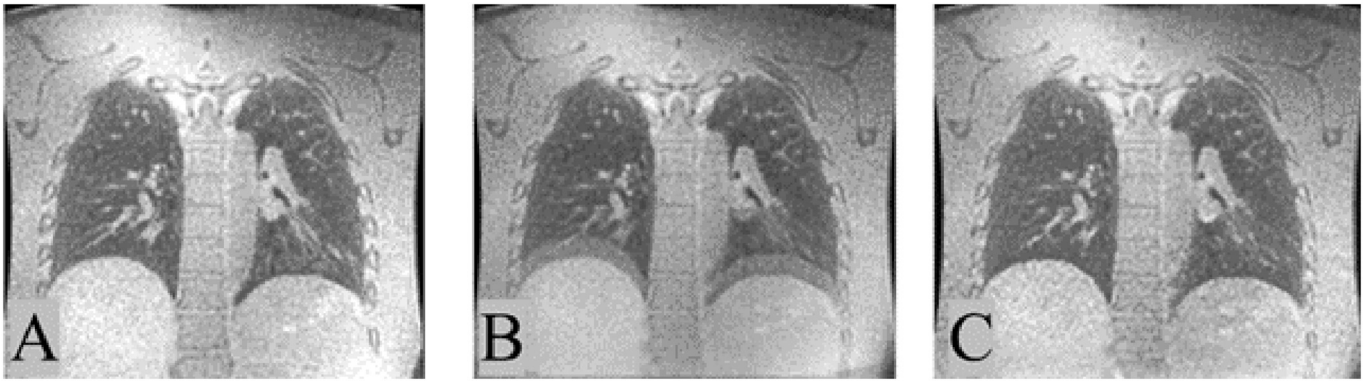

Fig. 7. Validation set. A is the ground truth (native ZTE-BH), B is the artificially modified BH images mimicking the ZTE4D artifacts, C is the prediction by the network.

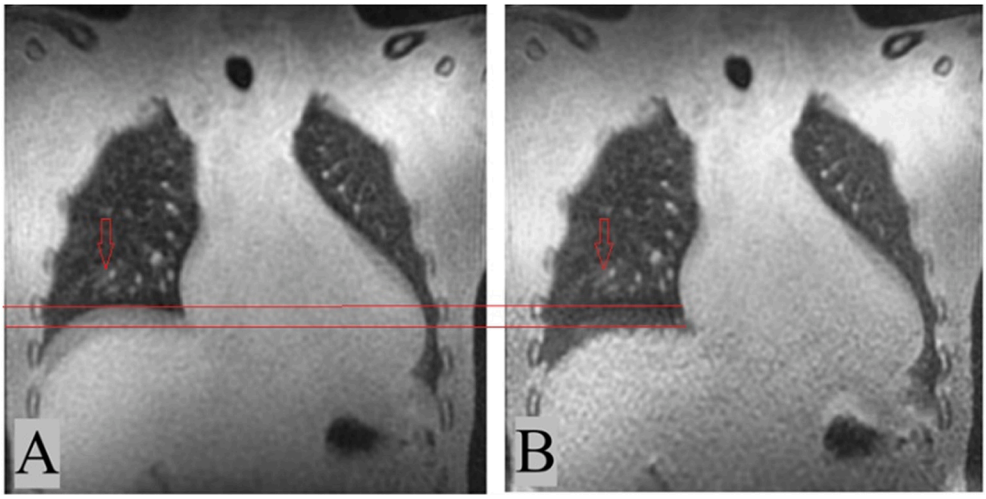

Fig. 8. Result of the prediction on unseen data. A is the unseen ZTE4D and B is the prediction by the network. Horizontal lines show the diaphragm positions, and the arrows point to a vessel getting enhanced by the network.

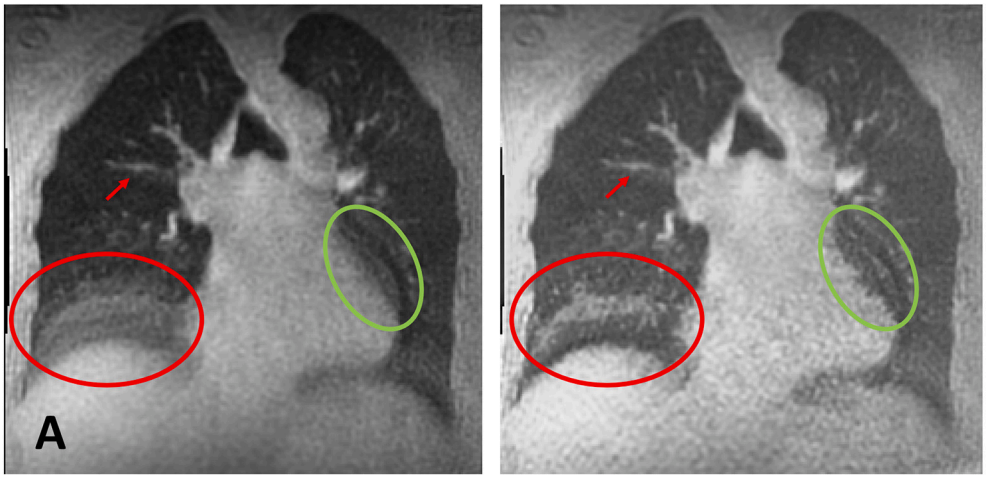

Fig. 9. ZTE4D original (A) and predicted (B) images of a volunteer with a very inconsistent breathing pattern. Red circles show the artefact from diaphragm movement, green ones highlight the blurring of the hearth. The red arrow shows an example vessel, which get sharper definition. Our model improved the images, finding sharp edges of the diaphragm, but it was unable to completely removing the movement artifacts. (For interpretation of the references to colour in this figure legend, the reader is referred to the web version of this article.)

$$SNR = \frac{SI_{lung\ parenchyma}}{STD_{trachea}}.$$

We choose this way to calculate SNR since the conventional method of taking the STD from the background air of the image was not possible, as the field of view (FOV) did not contain background air, or when it did, due to the shortness of the echo time, the coil elements became visible which was a major disturbance in the selection. As expected, this resulted in higher SNR values, due to the very low standard deviation of the signal inside the small area of the trachea.

CNR of the lung parenchyma and pulmonary artery - indicating visibility of intrapulmonary vessels – was also calculated. Calculations of

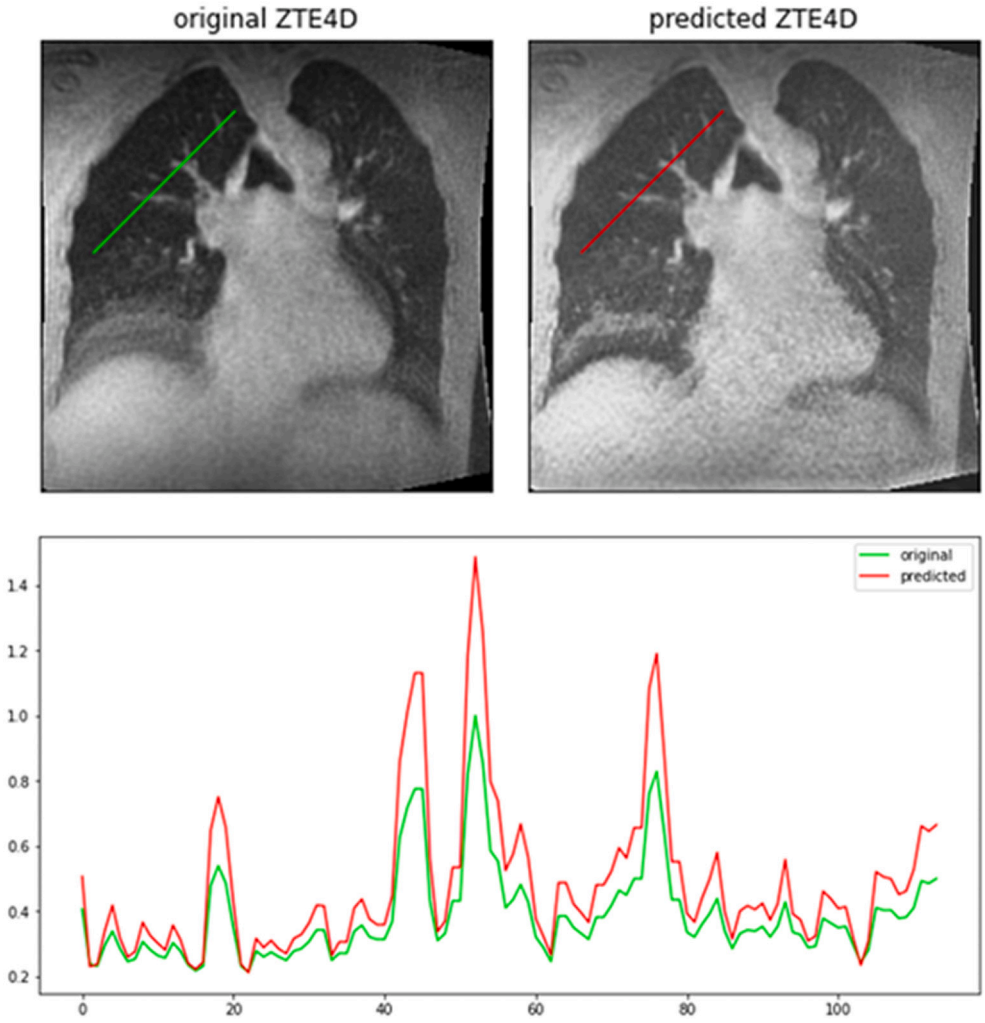

Fig. 10. Representation of the fine structure visualization with a line plot over intrapulmonary vessels. The curves show the signal intensities over the drawn lines on the original and the predicted ZTE4D images.

the CNR values were as follows:

$$\mathrm{CNR} = \frac{\mathrm{mean}(\mathrm{SI}\ (\mathrm{pulmonary\ artery}\ )\ ) - \mathrm{mean}\ (\mathrm{SI}\ (\mathrm{lung})\ )}{\mathrm{STD}(\mathrm{SI}\ (\mathrm{lung})\ )}.$$

The ROI in the lung parenchyma was carefully positioned and sized on the original scans to exclude any vessels. The ROIs of the vessels included pixels from pulmonary artery (see Fig. 5). For image segmentation ITK-SNAP was used [21].

3. Results

Our dataset contains MR scans from 10 healthy volunteers (age range 20–52, median 32). All subjects successfully completed the protocol.

Our model obtained an MSE of 0.09 on the training set and 0.135 on the validation set as shown on Fig. 6.

With quantitative assessment the ability of improving SNR was tested. Results are shown in Table 2.

The SNR values were improved almost by a factor of two, the CNR values by 4.2% ($p = 0.12$) by the FCNN.

The network successfully removed the diaphragm's motion artifacts from the validation set as illustrated in Fig. 7.

When tested on unseen data of ZTE4D the predicted images from our model improved the contrast of the pulmonary parenchyma against air filled regions (airways or air trapping). By visual inspection, it is obvious that artifacts like the shadowing diaphragm were considerably reduced, (Fig. 8.).

One of the biggest artifacts we see on the images was due to the diaphragm movement, mostly motion artefact at different inflation positions. The artefact was reduced by the network, and giving sharp edges for the diaphragm.

Figs. 9 and 10 are exemplary of the worst images obtained in the ZTE4D scans, when the volunteer's breathing pattern was inconsistent. Our model improved the image substantially, but some remaining artifacts were present.

The 16 different phases can be seen in the supplementary material.

4. Discussion

Currently, free-breathing technique is required for infants, pediatric patients below 6 years old or for patients who are incapable of following breath-hold instructions. The main advantage of using ZTE4D is the possibility to capture different both the inspiratory and the expiratory respiratory phases in a single examination [22]. ZTE4D has the potential of capturing 16 different respiratory phases to get information of the parenchymal signal changes together with the anatomical information. The main limitation of the current implementation of ZTE4D technique is that from all 16 phases only the end-expiratory ones are acceptable in term of image quality, mostly because inconsistent respiratory gating. Motion artifacts of the diaphragm, blurring of fine anatomical structures and lower SNR appear on most of the captured phases. In this study we

aimed to improve ZTE4D MR image quality using a FCNN, by removing possible motion artifacts related to breathing.

The first challenge of developing the image post processing pipeline was to create a training dataset. ZTE4D and ZTE3D-BH had the same parameters set, so firstly we tried to match the breath-hold images with the free-breathing ones. This was unsuccessful, as the volunteers were never laying completely still, and during tidal breathing the captured phases were not always matching any of the breath-hold phases. Since there were no ground truth for ZTE4D we created artificial ones from the breath-hold images. On the real ZTE4D images the diaphragm's motion artefact, blurring and increased noise level appear differently not just from patient to patient but within one patient as well between different respiratory phases. This indicated that not only the depths of motion artifacts of the diaphragm but also the distance of the movement varied. We took this into account and randomly changed the parameters image by image when we created the training dataset.

The SNR of the lung parenchyma was quantitatively improved by a factor of 1.98 and the CNR lung- blood, which is indicating the visibility of the intrapulmonary vessels, was improved by 4.2%. Our main goal was rather to remove the diaphragm's motion artifacts from the ZTE4D images, to improve diagnostic quality of the images. Our network was able to reduce these motion artifacts, such as diaphragm movement and blurring, and enhancing image quality. As main results of the network, diaphragm contour increased with sharper edges by visual inspection and less blurring of the anatomical structures and lung parenchyma.

Data leakage is a big problem in machine learning. This occurs, for example, when data from the same person is used to create the model and to validate the model [23]. In this study, apart from one individual, we tested the model on data from the same volunteers as it was trained on. However, ZTE3D BH and ZTE4D are different acquisitions, and a person is never 100% motionless plus the breathing pattern changes even if they are completely calm. This is the reason we considered that the ZTE4D scans of the five volunteers who were part of the training/validation sets were not related to their ZTE3D-BH scans, as they contain different information.

Our method shows still some limitations: the sample size is small and more data with an extended range of different artefact could be added to the training set to improve the method. To further improve the network, it could extend to different views and not only the coronal view, matching the usual axial radiological view. We plan to improve the performance including more volunteers and clinically validate it on patient data for its clinical acceptance.

5. Conclusion

We propose a post-processing pipeline to improve the image quality of ZTE4D in not-near end expiratory phases using a FCNN. We demonstrated that our method is allowing free breathing acquisition for better visualization of the lung parenchyma in various respiratory phases in subjects with irregular respiration pace.

Supplementary data to this article can be found online at https://doi.org/10.1016/j.mri.2023.01.019.

References

[1] Liszewski MC, Ciet P, Lee EY. MR imaging of lungs and airways in children. Magn Reson Imaging Clin N Am May 2019;27(2):201–25. https://doi.org/10.1016/j.mric.2019.01.002.

[2] Tiddens HAWM, et al. Respiratory tract exacerbations revisited: ventilation, inflammation, perfusion, and structure (VIPS) monitoring to redefine treatment. Pediatr Pulmonol Oct. 2015;50(Suppl. 40):S57–65. https://doi.org/10.1002/ppul.23266.

[3] Zucker EJ, Cheng JY, Haldipur A, Carl M, Vasanawala SS. Free-breathing pediatric chest MRI: performance of self-navigated golden-angle ordered conical ultrashort echo time acquisition. J Magn Reson Imaging JMRI Jan. 2018;47(1):200–9. https://doi.org/10.1002/jmri.25776.

[4] Bergin CJ, Glover GH, Pauly JM. Lung parenchyma: magnetic susceptibility in MR imaging. Radiology Sep. 1991;180(3):845–8. https://doi.org/10.1148/radiology.180.3.1871305.

[5] Macdougall RD, Strauss KJ, Lee EY. Managing radiation dose from thoracic multidetector computed tomography in pediatric patients: background, current issues, and recommendations. Radiol Clin North Am Jul. 2013;51(4):743–60. https://doi.org/10.1016/j.rcl.2013.04.007.

[6] Pearce MS, et al. Radiation exposure from CT scans in childhood and subsequent risk of leukaemia and brain tumours: a retrospective cohort study. Lancet Lond Engl Aug. 2012;380(9840):499–505. https://doi.org/10.1016/S0140-6736(12)60815-0.

[7] Ciet P, et al. Magnetic resonance imaging in children: common problems and possible solutions for lung and airways imaging. Pediatr Radiol 2015;45(13):1901–15. https://doi.org/10.1007/s00247-015-3420-y.

[8] Bae K, et al. Comparison of lung imaging using three-dimensional ultrashort echo time and zero echo time sequences: preliminary study. Eur Radiol May 2019;29(5):2253–62. https://doi.org/10.1007/s00330-018-5889-x.

[9] Lewis CE, Prato FS, Drost DJ, Nicholson RL. Comparison of respiratory triggering and gating techniques for the removal of respiratory artifacts in MR imaging. Radiology Sep. 1986;160(3):803–10. https://doi.org/10.1148/radiology.160.3.3737921.

[10] Kumar S, et al. Feasibility of free breathing lung MRI for radiotherapy using non-Cartesian k-space acquisition schemes. Br J Radiol Dec. 2017;90(1080). https://doi.org/10.1259/bjr.20170037. 20170037.

[11] Bae K, et al. Respiratory motion–resolved four-dimensional zero echo time (4D ZTE) lung MRI using retrospective soft gating: feasibility and image quality compared with 3D ZTE. Eur Radiol Sep. 2020;30(9):5130–8. https://doi.org/10.1007/s00330-020-06890-x.

[12] Do S, Song KD, Chung JW. Basics of deep learning: a Radiologist's guide to understanding published radiology articles on deep learning. Korean J Radiol Jan. 2020;21(1):33–41. https://doi.org/10.3348/kjr.2019.0312.

[13] Long J, Shelhamer E, Darrell T. Fully convolutional networks for semantic segmentation. In: 2015 IEEE conference on computer vision and pattern recognition (CVPR); Jun. 2015. p. 3431–40. https://doi.org/10.1109/CVPR.2015.7298965.

[14] Simonyan K, Zisserman A. Very deep convolutional networks for large-scale image recognition. arXiv. Accessed: Jul. 28, 2022. [Online]. Available: http://arxiv.org/abs/1409.1556; Apr. 10, 2015.

[15] Han C, Duan Y, Tao X, Lu J. Dense convolutional networks for semantic segmentation. IEEE Access 2019;7:43369–82. https://doi.org/10.1109/ACCESS.2019.2908685.

[16] Henkelman RM. Measurement of signal intensities in the presence of noise in MR images. Med Phys Apr. 1985;12(2):232–3. https://doi.org/10.1118/1.595711.

[17] Ouahabi A. A review of wavelet denoising in medical imaging. In: 2013 8th international workshop on systems, signal processing and their applications (WoSSPA); May 2013. p. 19–26. https://doi.org/10.1109/WoSSPA.2013.6602330.

[18] Souza R, Frayne R. A hybrid frequency-domain/image-domain deep network for magnetic resonance image reconstruction. In: 2019 32nd SIBGRAPI conference on graphics, patterns and images (SIBGRAPI), Rio de Janeiro, Brazil; Oct. 2019. p. 257–64. https://doi.org/10.1109/SIBGRAPI.2019.00042.

[19] Souza R. Hybrid-CS-Model-MRI. Accessed: Nov. 02, 2022. [Online]. Available: https://github.com/rmsouza01/Hybrid-CS-Model-MRI; Sep. 14, 2022.

[20] josemanuel097/FBL_4DZTE_improvement. https://github.com/josemanuel097/FBL_4DZTE_improvement; 2022 (accessed Jul. 28, 2022).

[21] Yushkevich PA, et al. User-guided 3D active contour segmentation of anatomical structures: significantly improved efficiency and reliability. NeuroImage Jul. 2006;31(3):1116–28. https://doi.org/10.1016/j.neuroimage.2006.01.015.

[22] Iwasawa T, et al. Correlation of lung parenchymal MR signal intensity with pulmonary function tests and quantitative computed tomography (CT) evaluation: a pilot study. J Magn Reson Imaging JMRI Dec. 2007;26(6):1530–6. https://doi.org/10.1002/jmri.21183.

[23] Nayak SK, Ojha AC. Data leakage detection and prevention: review and research directions. 2020. https://doi.org/10.1007/978-981-15-1884-3_19.